

Discovery of the 5 keV cyclotron line followed by three harmonics in Swift J1626.6-5156

S. MOLKOV,^{1,2} V. DOROSHENKO,³ A. LUTOVINOV,^{1,2} S. TSYGANKOV,^{4,1} A. SANTANGELO,³ I. MEREMINSKIY,¹ AND A. SEMENA¹

¹*Space Research Institute, Russian Academy of Sciences, Profsoyuznaya 84/32, 117997 Moscow, Russia*

²*Moscow Institute of Physics and Technology, Moscow region, 141701 Dolgoprudnyi, Russia*

³*Institute for Astronomy and Astrophysics, University of Tübingen, Sand 1, 72026 Tübingen, Germany*

⁴*Department of Physics and Astronomy, FI-20014 University of Turku, Finland*

(Received XXX, 2021; Revised XXX, 2021; Accepted 17 June, 2021)

Submitted to ApJL

ABSTRACT

We report on observations of the Be/X-ray binary system Swift J1626.6-5156 performed with *NuSTAR* during a short outburst in March 2021, following its detection of by the *MAXI* monitor and Spektrum-Roentgen-Gamma (*SRG*) observatory. Our analysis of the broadband X-ray spectrum of the source confirms the presence of two absorption-like features at energies $E \sim 9$ and $E \sim 17$ keV previously reported in literature and interpreted as the fundamental cyclotron resonance scattering feature (CRSF) and its first harmonic (based on *RXTE* data). The better sensitivity and energy resolution of *NuSTAR*, combined with the low energy coverage of *NICER*, allowed us to detect two additional absorption-like features at $E \sim 4.9$ keV and $E \sim 13$ keV. We conclude, therefore, that in total four cyclotron lines are observed in the spectrum of Swift J1626.6-5156: the fundamental CRSF at $E \sim 4.9$ keV and three higher spaced harmonics. This discovery makes Swift J1626.6-5156 the second accreting pulsar, after 4U 0115+63, whose spectrum is characterized by more than three lines of a cyclotronic origin, and implies the source has the weakest confirmed magnetic field among all X-ray pulsars $B \sim 4 \times 10^{11}$ G. This discovery makes Swift J1626.6-5156 one of prime targets for the upcoming X-ray polarimetry missions covering soft X-ray band such as IXPE and eXTP.

Keywords: pulsars: individual (Swift J1626.6-5156) – stars: neutron – X-rays: binaries

1. INTRODUCTION

Swift J1626.6-5156 is a transient X-ray pulsar (XRP) with a spin period of ~ 15 s discovered on December 18, 2005 by the Swift Burst Alert Telescope (BAT) during a giant outburst (Krimm et al. 2005). The outburst lasted for approximately half a year and was followed by a longer period of a few years during which the object remained active and strongly variable on timescales from 45 to 95 days (Reig et al. 2008; Baykal et al. 2010).

The most complete study of the system to date has been conducted by Reig et al. (2011), who based on multi-frequency observations concluded that Swift J1626.6-5156 is a Be/X-ray binary (BeXRB) with

a B0Ve companion located at a distance of $D \sim 10$ kpc. This estimate is rather uncertain and also the Gaia EDR3 estimates are in the range of 5.8-12 kpc (Bailer-Jones et al. 2021). Here we adopt 10 kpc distance for easier comparison with previous results. The counterpart (2MASS16263652-5156305) shows strong $H\alpha$ emission (Negueruela & Smith 2006), typical of a Be star. The ~ 15.3 s spin period of the neutron star (Palmer et al. 2005; Markwardt & Swank 2005) and the 132.9 days orbital binary period (Baykal et al. 2010) are also typical for Be-systems (see e.g. Corbet 1986). At the same time, the binary orbit is near circular unlike most other BeXRBs. The optical counterpart is also rather faint in the infrared for a Be star (Rea et al. 2006). Finally, the observed outburst light curve is also not typical for Be/X-ray binaries, so the system is not without peculiarities.

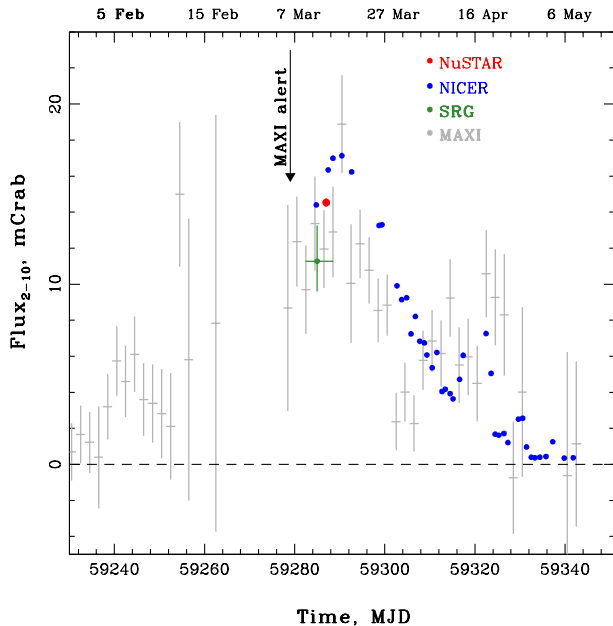


Figure 1. The *MAXI* light curve of Swift J1626.6-5156 around the 2021 outburst (grey crosses). On top of this curve fluxes obtained from the *NuSTAR* (red point) and *NICER* (blue points) data are presented. All fluxes are given in mCrab units in the 2 – 10 keV energy band. Date of the *MAXI* outburst trigger is shown with vertical arrow.

In the X-ray band the source was extensively studied using RXTE observations. The main result was a significant detection in the energy spectra of two cyclotron resonance scattering features (CRSFs) at $E \sim 10$ keV and $E \sim 18$ keV (DeCesar et al. 2013), which implied a magnetic field of $\sim 10^{12}$ G in the line forming region.

In 2008 the pulsar went into a low state characterised by a lowest observed luminosity of $\sim (3-4) \times 10^{33}$ erg s $^{-1}$ in the 0.5-10 keV energy band (Tsygankov et al. 2017) and remained undetected by all-sky monitors until 2021. On March 2021, *MAXI*/GSC significantly detected the source (Negoro et al. 2021a), suggesting that Swift J1626.6-5156 had started a new giant outburst after fifteen years of relative quiescence (Fig. 1). However, in the following few weeks, no giant outburst developed and only a modest flux enhancement was observed (Molkov et al. 2021). Moreover, the analysis of archival *MAXI* data revealed that the source actually shows flaring activity from time to time (Negoro et al. 2021b), i.e. confirming likely accretion in quiescence (Tsygankov et al. 2017).

Here we report results of observations of Swift J1626.6-5156 performed in March 2021 with the *SRG*, *NuSTAR*, and *NICER* missions covering a broad energy range from 0.2 to 78 keV.

2. OBSERVATIONS AND DATA REDUCTION

As already mentioned, Swift J1626.6-5156 remained in a state of relative quiescence until 2021, after the end of the giant outburst and following activity in 2005-2008. First evidence for a renewed activity of the source was reported by (Negoro et al. 2021a) using *MAXI* (Matsuoka et al. 2009) data. Initially, it was proposed that the source was entering into a new giant outburst, but the follow-up monitoring campaigns revealed that this was not the case.

To follow the flux evolution of the source in this flare, we used publicly available data from *MAXI*¹. The resulting light curve re-binned to 2 day time intervals is shown on Fig. 1, where all fluxes are given in mCrab units in the 2 – 10 keV range. The source flux measured with the Neutron star Interior Composition Explorer (*NICER*, Gendreau & Arzoumanian 2017) is plotted in the same figure. The public data were downloaded from the HEASARC archive system and processed with HEASOFT v.6.28, using the *NICER* Calibration Database (CALDB) version 20200722. For background estimation we used the NIBACKGEN3C50 tool.

As shown in Fig. 1, *NICER* performed many observations covering a large part of the outburst of 2021. Since in this article we focus on the broadband spectral analysis, we only report the analysis of the first observation (ID:4202070101) performed on Mar. 11, 2021, temporally close and at similar flux level of the *NuSTAR* observation (see below).

We used data obtained by the *SRG* observatory (Sunyaev et al. 2021) during the third all sky survey to assess source flux at early stages of the outburst and improve the low-energy coverage for phase-averaged spectra (Fig. 1). The sky region around Swift J1626.6-5156 was scanned by *SRG* on Mar 12, 2021. Both the *Mikhail Pavlinsky* ART-XC telescope (Pavlinsky et al. 2021) and the eROSITA telescope (Predehl et al. 2021) onboard the *SRG* observatory detected the source with the high significance (Molkov et al. 2021). The source flux in the 2-10 keV energy band resulted from the joint fit of the ART-XC and eROSITA spectra is shown in Fig. 1.

Based on the above data we requested follow-up observations with the *NuSTAR* (Nuclear Spectroscopic Telescope ARray) observatory. It consists of two X-ray telescope modules, to which we refer to as FPMA and FPMB (Harrison et al. 2013). It provides X-ray imaging, spectroscopy and timing in the energy range of 3-

¹ http://maxi.riken.jp/star_data/J1626-519/J1626-519.html.

Data are multiplied by 2 because of about half the sky region to obtain the fluxes is masked to avoid count leaks from a nearby source (Negoro et al. 2021a)

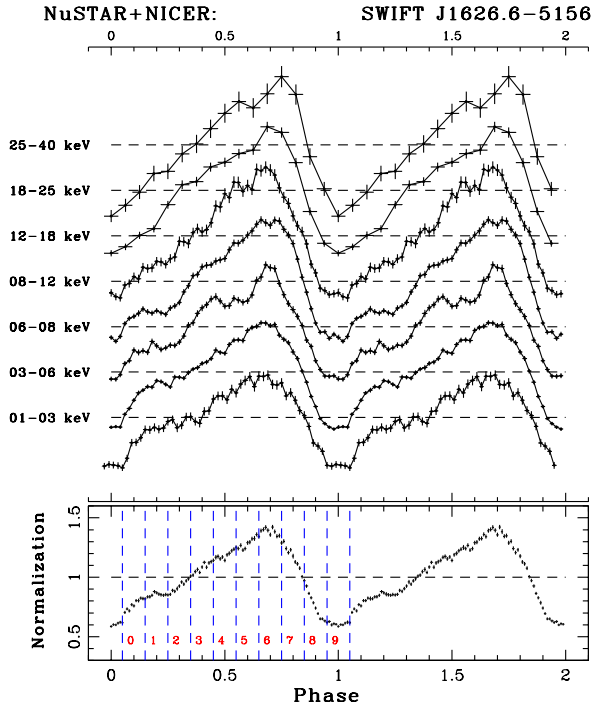


Figure 2. Energy-resolved pulse profiles of Swift J1626.6-5156 obtained with *NuSTAR* (above 3 keV) and *NICER* (1-3 keV). On the bottom panel an averaged *NuSTAR* pulse profile in the 3-50 keV energy band is shown. Vertical lines define boundaries of phase bins selected for spectral analysis.

79 keV with an angular resolution of $18''$ (FWHM) and spectral resolution of 400 eV (FWHM) at 10 keV. *NuSTAR* performed one observation of Swift J1626.6-5156 on Mar 13-14, 2021, near the peak of the flare (ObsIDs:90701311002) with the on-source exposure of ~ 56 ks (see Fig. 1). *NuSTAR* data were processed with the standard *NuSTAR* Data Analysis Software (NUSTAR-DAS_19JUN20_v2.0.0) provided under HEASOFT v6.28 with CALDB version 20201217.

All *NuSTAR* and *NICER* spectra were grouped to have at least 25 counts per bin and at least 3 detector channels, to ensure that the binning of the spectra matches the energy resolution of the detectors. The final data analysis (timing and spectral) was performed with the HEASOFT 6.28 software package. All uncertainties are quoted at the 1σ confidence level, if not stated otherwise.

3. RESULTS

In this section we present the detailed results of spectral (including pulse phase-resolved) and timing analysis of *NuSTAR* and *NICER* data.

3.1. Energy-resolved pulse profile

The orbital ephemerides for Swift J1626.6-5156 are not well known (see [I^cdem et al. 2011](#), and references therein). This is not relevant for the current work as the duration of the *NuSTAR* observation is much shorter than the expected orbital period. Therefore only barycentric correction was applied to the light curves and the pulse period of $P = 15.33962(1)$ s used for phase-resolved spectroscopy was determined. Uncertainty for the pulse period value was calculated from the Monte-Carlo simulations ([Boldin et al. 2013](#)).

Energy resolved pulse profiles obtained with *NuSTAR* in the 3 – 40 keV energy interval and with *NICER* in the 1 – 3 keV energy interval, folded with the aforementioned period are presented in Fig. 2. Phase '0' corresponds to the minimum of the light curve folded in the whole *NuSTAR* energy band. The source pulse profile is mainly characterized by one rather broad peak and demonstrates some evolution of both the shape and pulsed amplitude with the phase. In particular in softer energies, the profile shows two sub-peaks near phases 0.1 and 0.4. As the energy increases the features disappear.

The pulsed fraction gradually increases with the energy from $\sim 40\%$ at 3 – 5 keV to $\sim 60\%$ at 30 – 40 keV (Fig. 3). Such a behaviour is typical for the majority of bright XRPs (see, e.g., [Lutovinov & Tsygankov 2009](#)). Furthermore, a sharp decrease of the pulsed fraction is observed around 20 keV, that roughly corresponds to the energy of the cyclotron line harmonic reported by [DeCesar et al. \(2013\)](#). Hints of decrease in the pulse fraction are also observed around ~ 10 keV, reported by those authors as a fundamental energy of cyclotron line, and at even lower energies, i.e., below 10 keV. The counting statistics do not allow making any significant conclusions. It is worthy to note that very similar decrease of the pulsed fraction near the first harmonic of the cyclotron line was early found by [Ferrigno et al. \(2009\)](#) in 4U 0115+63. Both these findings are quite rare as an increase of the pulsed fraction is usually observed near the cyclotron line and its harmonics (see, e.g., [Tsygankov et al. 2007](#); [Lutovinov & Tsygankov 2009](#); [Shtykovsky et al. 2019](#)).

3.2. Phase-averaged spectrum

The spectrum of Swift J1626.6-5156 is typical for accreting XRPs (see, e.g., [Nagase 1989](#); [Filippova et al. 2005](#)). It is characterized by an exponential cutoff at high energies (Fig. 4), that can be explained in terms of the Comptonization processes in hot emission regions (see, e.g., [Sunyaev & Titarchuk 1980](#); [Meszaros & Nagel 1985](#); [Titarchuk 1994](#)). We modelled the broadband continuum spectrum with two commonly used phenomenological models: a power law with

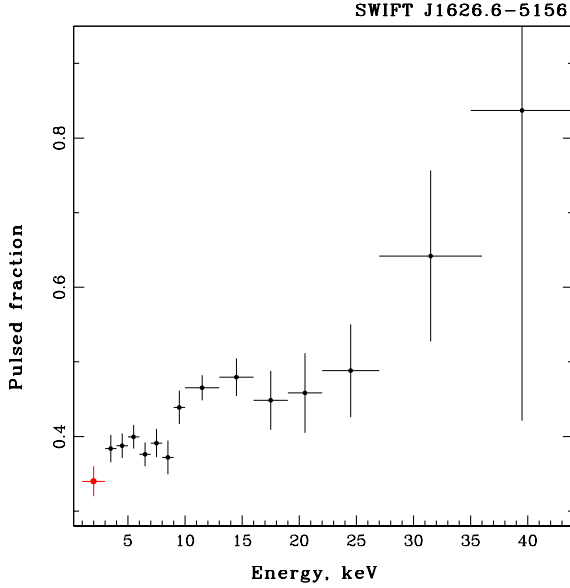


Figure 3. Dependence of the pulsed fraction of Swift J1626.6-5156 on the energy. NuSTAR values shown by black color, NICER 1-3 keV measurement – in red.

an exponential cutoff (`cutoffpl` in the XSPEC package, hereafter `model1`) and a thermal Comptonization model (`comptt`, hereafter `model2`). To take into account the uncertainty in calibrations of two modules of *NuSTAR* a cross-calibration constant C_{modB} was included in all spectral fits. Furthermore, two cross-calibration constants were added for *NICER* (C_{NIC}), and eROSITA (C_{eRo}) spectra, to compensate for some flux difference between the observations by these instruments (we assume that the spectrum shape does not change significantly). Depending on the continuum model, the inclusion of a soft black body component with the temperature of ~ 0.1 keV improves the fit quality in the softer part of the spectrum (see also, Iwakiri et al. 2021). We included in the fit a Gaussian function to model an emission of the neutral fluorescence iron line (`gauss`), and the `phabs` component to take into account interstellar absorption. For both continua, an inclusion of two earlier reported absorption features around 10 and 20 keV was also necessary to obtain a meaningful fit (`gabs`). Results of the fit are presented in Fig. 4a and Table. 1.

The quality of the fit is however not acceptable for both models. Although the reduced χ^2 value is around ~ 1.2 for `model2`, an assessment of the fit quality using simulations (by means of a `goodness` command in Xspec) revealed an unsatisfactory quality of the fit (Table 1). Poor quality of the fit is also revealed by residuals which are observed around 5 and 13 keV (Fig. 4b,c).

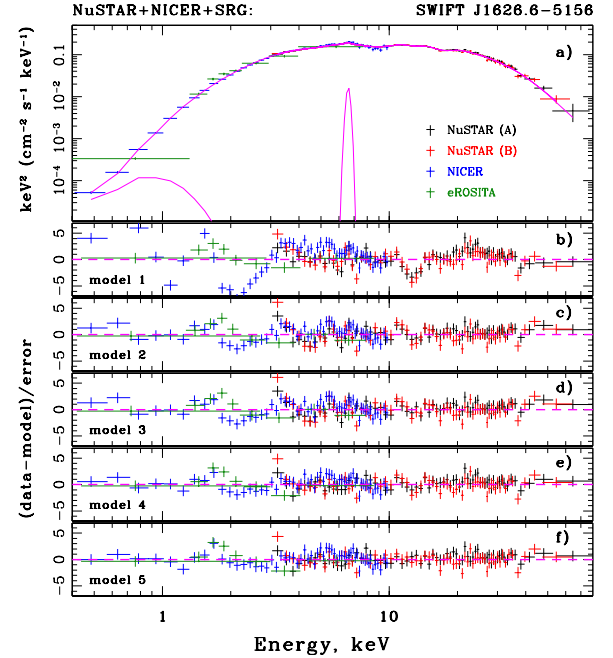


Figure 4. The phase-averaged energy spectrum of Swift J1626.6-5156 reconstructed in a wide energy range with the *NuSTAR*, *NICER* and *SRG*/eROSITA instruments (upper panel). The five bottom panels show residuals for the five spectral models (see the text and Table 1).

The quality of the fit could be improved by including additional absorption line features near 13 keV (`model3`, Fig. 4d) or near 5 keV (`model4`, Fig. 4e). We note, however, that including only one of the two lines does not result in a statistically acceptable fit. If we add only a 13 keV line then neither fit-statistic nor Bayesian information criteria (appropriate for comparison of non-nested models) indicate significant improvement and the goodness parameter remains at an unacceptable level. Adding only the 5 keV absorption feature leads to better approximation and goodness parameter becomes closer to 50%. But only the inclusion of both lines (`model5`) dramatically improves the quality of the fit (Fig. 4f) and makes it adequate both in terms of fit-statistics and Bayesian criteria, and as assessed with simulations using `goodness` command.

We finally conclude, therefore, that a statistically acceptable fit of the averaged spectrum can only be obtained if all four absorption features are included in the model. This, together with the fact that the centroid energies of these features appear to be harmonically spaced for a fundamental line energy at $E \sim 5$ keV, strongly indicates that all four features have a physical origin.

On the other hand, also the best-fit discussed above has some issues. As it can be seen in Table 1, the centroid of the iron line energy becomes significantly

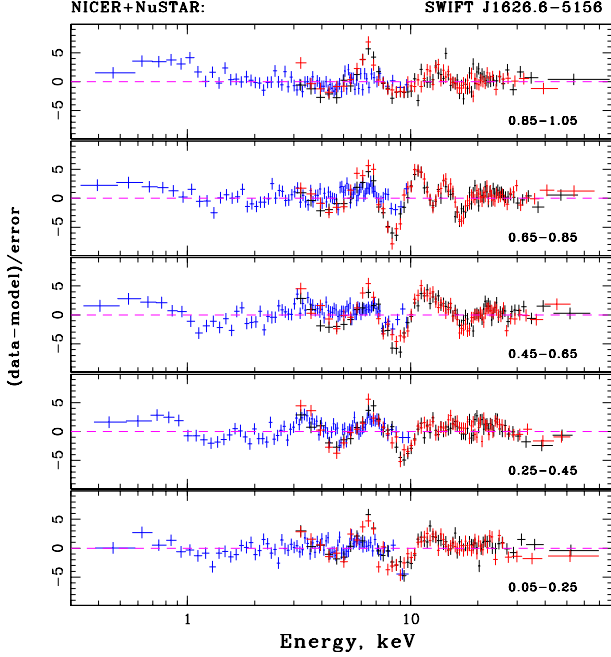


Figure 5. Residuals of the pulse-phase resolved joint *NICER* and *NuSTAR* spectra fitting with the absorbed Comptonization model (see text for detail). Phase intervals values are given in the each panel.

higher than the expected value of 6.4 keV in *model14* and *model15*. We note that the equivalent width of this line is quite low, which might imply that the available statistics actually does not allow to significantly detect the line and constrain its parameters, so the increase of its apparent energy might be an artifact of the fit. Indeed, the shifted energy of the iron line appears in models with the addition of the soft absorption feature at $E \sim 5$ keV (*model14* and *model15*). Taking into account that the both models contain an absorption line around $E \sim 9$ keV, one can imagine the appearance of the emission-like feature in the region around 6-7 keV, especially if the centroid energies of these absorption features vary with the pulse phase. To investigate this issue in detail, we performed also the phase-resolved spectral analysis.

3.3. Pulse phase-resolved spectroscopy

It is well established that spectra of XRPs vary with the pulse phase. Parameters of the cyclotron resonant scattering features (CRSFs) are also known to change at such time scales (see, e.g., Burderi et al. 2000; Kreykenbohm et al. 2004; Heindl et al. 2004; Lutovinov et al. 2015, and references therein), and, in some cases, lines can only appear significantly at certain phase intervals (Molkov et al. 2019). Therefore the

pulse phase-resolved spectroscopy can be considered as a tool for the study of the line properties, and ultimately for probing the geometry of the emission regions in the vicinity of the neutron star and its magnetic field structure. Here we focus on understanding whether the absorption features are detected at individual pulse phases in order to exclude the situation when the detection of the features in the averaged spectrum arises from the modeling of superimposed spectra variable across different pulse phases.

As a first step, we fitted phase-resolved *NuSTAR* and *NICER* spectra extracted from the 0.2 phase length intervals with the Comptonization model continuum modified by the interstellar absorption but without absorption or emission like features and soft black-body component. Residuals of the fits relative to the absorption lines (Fig. 5) are observed throughout the pulse, although the depth of the individual features appears to be variable and is most clearly seen at the phase interval 0.65-0.85.

On the next step, we fitted these spectra adding up to four absorption-like features. Unlike to the phase-averaged analysis, we did not include the soft black body component (fits are not sensitive to that, probably due to the lack of statistics in phase-resolved spectra) and the iron line. At all phases, the inclusion of the two absorption features at $E \sim 5$ keV and $E \sim 9$ keV is necessary to obtain significant fits. For phases 0.05 – 0.25 and 0.25 – 0.45 these two components are actually sufficient. For phases 0.45 – 0.65 and 0.85 – 1.05 the inclusion of an additional absorption line at $E \sim 17$ keV strongly improves the fit quality. In first case, the value of the χ^2 changes from 730 (650 dof) to 681 (647 dof), and in the second, from 671 (579 dof) to 644 (576 dof). In terms of Bayesian criteria, we obtain $\Delta BIC = 41$ and $\Delta BIC = 19$ for the first and the second cases, respectively, which implies (since both values are > 10) that the strength of statement that the model with three lines is better than with two lines is “Very strong”. Finally, to achieve an acceptable fit for the spectrum at phase 0.65 – 0.85, all four absorption lines have to be included. More specifically, the χ^2 value changes from 796 (660 dof) to 704 (657 dof) after adding the line at ~ 17 keV, and reduces to 630 (564 dof) after a fourth absorption line feature at ~ 13 keV is included (see Fig. 6). Bayesian information criterion decreases on 83 and 65, respectively. Results of the approximation of the phase-resolved spectra are summarized in Table 2.

Thus we have confirmed presence of all four absorption features in the phase-resolved spectra as well. However, not all lines are detected in all phase bins. We also note that their energies vary slightly with the pulse phase. In addition, we note that to describe the phase-resolved

Table 1. Best-fitting results for the Swift J1626.6-5156 averaged-spectrum for five models

	model1 pha × (bb+cutoff+ga) ×2 gabs	model2 pha × (bb+comptt+ga) ×2 gabs	model3 pha × (bb+comptt+ga) ×3 gabs	model4 pha × (bb+comptt+ga) ×3 gabs	model5 pha × (bb+comptt+ga) ×4 gabs
Parameter	Value	Value	Value	Value	Value
N_H ^a	2.23 ± 0.02	0.77 ± 0.03	0.78 ± 0.03	0.61 ± 0.04	0.42 ± 0.05
kT_{BB} , keV	0.08 ± 0.01	0.14 ± 0.01	0.14 ± 0.01	0.14 ± 0.01	0.13 ± 0.03
A_{BB} ^b , ×10 ³	654 ± 92	0.33 ± 0.06	0.34 ± 0.07	0.27 ± 0.03	0.03 ± 0.01
Γ	1.14 ± 0.01	—	—	—	—
E_{fold} , keV	10.12 ± 0.12	—	—	—	—
A_{cut} ^c , ×10 ¹	0.67 ± 0.01	—	—	—	—
T_0 , keV	—	0.89 ± 0.01	0.89 ± 0.01	0.99 ± 0.02	1.17 ± 0.08
T_p , keV	—	5.36 ± 0.04	5.32 ± 0.04	5.65 ± 0.07	5.74 ± 0.16
τ_p	—	4.22 ± 0.04	4.26 ± 0.04	3.83 ± 0.08	3.43 ± 0.25
A_{comp} , ×10 ¹	—	0.156 ± 0.002	0.157 ± 0.002	0.148 ± 0.002	0.157 ± 0.005
E_{Fe} , keV	6.38 ± 0.05	6.41 ± 0.03	6.41 ± 0.03	6.57 ± 0.03	6.59 ± 0.03
σ_{Fe} , keV	0.61 ± 0.05	0.46 ± 0.03	0.46 ± 0.03	0.16 ± 0.05	0.13 ± 0.05
A_{Fe} ^d , ×10 ³	0.64 ± 0.07	0.58 ± 0.05	0.58 ± 0.05	0.18 ± 0.03	0.16 ± 0.04
EW_{Fe} , eV	146	142	141	42	32
E_{cyc1} , keV	—	—	—	4.73 ± 0.05	4.82 ± 0.05
σ_{cyc1} , keV	—	—	—	0.58 ± 0.09	0.93 ± 0.09
τ_{cyc1} , keV	—	—	—	0.12 ± 0.03	0.47 ± 0.14
E_{cyc2} , keV	9.02 ± 0.06	8.94 ± 0.04	8.95 ± 0.05	8.78 ± 0.05	8.63 ± 0.06
σ_{cyc2} , keV	1.18 ± 0.08	0.77 ± 0.06	0.79 ± 0.06	1.00 ± 0.07	1.74 ± 0.20
τ_{cyc2} , keV	0.45 ± 0.03	0.21 ± 0.02	0.22 ± 0.02	0.38 ± 0.05	1.51 ± 0.56
E_{cyc3} , keV	—	—	12.96 ± 0.20	—	12.84 ± 0.11
σ_{cyc3} , keV	—	—	0.57 ± 0.26	—	0.97 ± 0.15
τ_{cyc3} , keV	—	—	0.06 ± 0.03	—	0.30 ± 0.11
E_{cyc4} , keV	17.00 ± 0.11	17.33 ± 0.10	17.37 ± 0.10	17.21 ± 0.10	17.09 ± 0.14
σ_{cyc4} , keV	1.06 ± 0.11	1.28 ± 0.11	1.45 ± 0.13	1.02 ± 0.11	1.65 ± 0.21
τ_{cyc4} , keV	0.37 ± 0.04	0.52 ± 0.05	0.63 ± 0.07	0.38 ± 0.04	0.82 ± 0.18
C_{modB}	1.064 ± 0.003	1.064 ± 0.003	1.064 ± 0.003	1.064 ± 0.003	1.064 ± 0.005
C_{NIC}	0.917 ± 0.005	0.944 ± 0.005	0.944 ± 0.005	0.946 ± 0.005	0.948 ± 0.005
C_{eRo}	0.772 ± 0.003	0.802 ± 0.003	0.802 ± 0.003	0.804 ± 0.003	0.805 ± 0.003
F_X ^e , ×10 ¹⁰	5.5	5.5	5.5	5.5	5.5
χ^2 (d.o.f.)	1604.0 (864)	1027.6 (863)	1015.4 (860)	930.3 (860)	906.9 (857)
goodness	100%	99%	99%	74%	54%
BIC	1657	1084	1080	995	981
Δ BIC	—	—	$BIC_{model2} - BIC_{model3} = 4$	$BIC_{model2} - BIC_{model4} = 89$	$BIC_{model4} - BIC_{model5} = 14$

Notes. Here N_H is the column density, kT_{BB} is the black-body temperature, Γ is the power-law photon index, E_{fold} is the folding energy of the cutoff power law. T_0 , T_p and τ_p are the seed photons temperature, the plasma temperature and the plasma optical depth Comptonization model parameters. E_{Fe} , σ_{Fe} and EW_{Fe} are the iron line energy, width and equivalent width, respectively. E_{cyc} , σ_{cyc} and τ_{cyc} are the energy, width and optical depth of cyclotron lines.

^a Value of N_H is in units of 10^{22} atom cm^{-2}

^b Normalization parameter calculated as L_{39}/D_{10}^2 , where L_{39} is the source luminosity in units of 10^{39} erg/s and D_{10} is the distance to the source in units of 10 kpc

^c Units are $photons\ keV^{-1}\ cm^{-2}\ s^{-1}$ at 1 keV

^d Total $photons\ cm^{-2}\ s^{-1}$ in the line

^e Model flux in the 3-50 keV energy band in units of $erg\ cm^{-2}\ s^{-1}$.

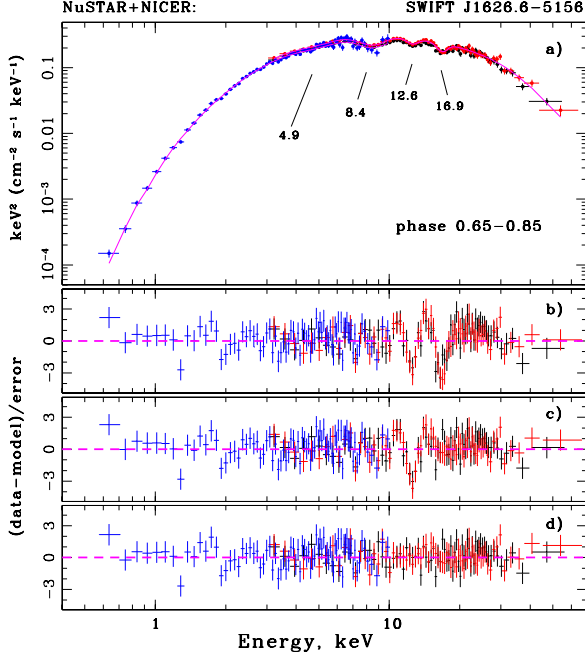


Figure 6. (a) The energy spectrum of Swift J1626.6-5156 at the pulse phases 0.65-0.85 reconstructed with *NuSTAR* and *NICER* and fitted with the Comptonization model modified by interstellar absorption and four absorption features (see the text for details). Residuals for spectral model: without two absorption lines with the highest energies (b), including line near 17 keV (c) and including all lines (d).

spectra, it is not necessary to include a component for the iron line.

4. DISCUSSION AND CONCLUSIONS

Most of the known cyclotron line sources exhibit either only the fundamental CRSF or the fundamental one and its first harmonic. This is likely a selection effect associated with the difficulty of detecting such features at higher energies. In fact, most accreting pulsars are strongly magnetized with fundamental line energies typically above the a cutoff energy at around 20 keV (see e.g., [Staubert et al. 2019](#) for a recent review). The detection of the first and certainly of the second harmonics is challenging due to the lack of photons well above the cutoff.

In our analysis, we not only confirm the CRSFs at 8.6 and 17.1 keV in the spectrum of Swift J1626.6-5156 already reported in literature, but also discover two additional features around ~ 4.9 keV and ~ 13 keV. We conclude, therefore, that four CRSFs characterize the spectrum of Swift J1626.6-5156, with the fundamental line at $E \sim 4.9$ keV, and other three features being harmonics of this feature. This implies that Swift J1626.6-5156 has the lowest confirmed magnetic field among

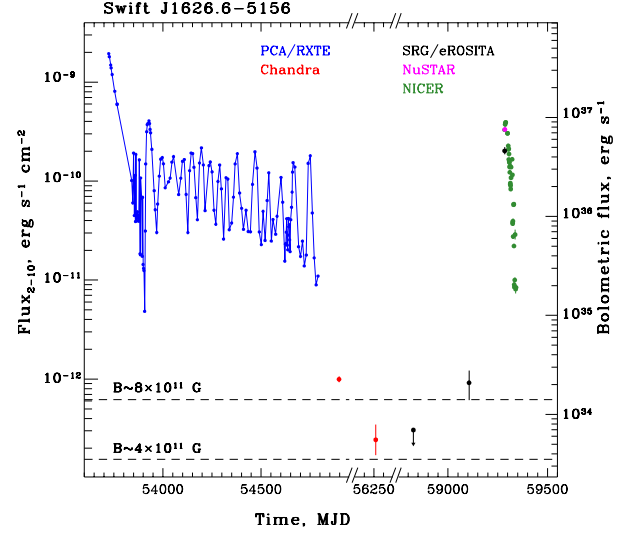


Figure 7. Swift J1626.6-5156 long-term flux history. Bolometric luminosity calculated in assumption of 10 kpc distance to the source. Dashed lines show luminosity when the source should drop to the propeller regime for two magnetic field values corresponding to 4.9 and 9 keV fundamental cyclotron lines.

all X-ray pulsars, and is only second to 4U 0115+63 ([Santangelo et al. 1999](#)) by total number of observed cyclotron lines.

In the case of Swift J1626.6-5156 the detection of four lines is only possible due to the low energy of the fundamental one. The strength of the neutron star magnetic field is thus estimated to be $B \sim 4.1(1+z) \times 10^{11}$ G. The only other XRP with the comparable field is the peculiar “bursting pulsar” GRO J1744-28 ([Doroshenko et al. 2015](#); [D’Ai et al. 2015](#)). Our result is rather unexpected and it is interesting to compare the magnetic field strength estimated through the CRSF with other indirect estimates.

First, as already mentioned, we note that the source continues to accrete in quiescence ([Tsygankov et al. 2017](#)) down to a bolometric luminosity of $\simeq 5.9 \times 10^{33} d_{10}^2 \text{ erg s}^{-1}$ (here we recalculated the lowest observed luminosity in the 0.5-10 keV energy band to the bolometric one based on our knowledge of the source broad band spectrum and d_{10} is distance to the source scaled to 10 kpc). This is consistent with the observed eROSITA flux and the source flux variability at low luminosities as illustrated by Fig. 7. If the accretion continues, then the lowest luminosity value must have been higher than the limiting luminosity for the transition to the propeller regime ([Tsygankov et al. 2016](#)):

$$L_{lim} = 4 \times 10^{37} k^{7/2} B_{12}^2 P^{-7/3} M_{1.4}^{-2/3} R_6^5 \leq L_{10} d_{10}^2$$

Table 2. Best-parameters of the Swift J1626.6-5156 phase-resolved spectra fitting with the Comptonization model modified by interstellar absorption and with inclusion of up to four cyclotron-line absorption features

<i>phase</i>	0.05-0.25	0.25-0.45	0.45-0.65	0.65-0.85	0.85-1.05
Parameter	Value	Value	Value	Value	Value
N_{H}	0.37 ± 0.02	0.44 ± 0.03	0.43 ± 0.02	0.42 ± 0.02	0.28 ± 0.03
T_0 , keV	1.14 ± 0.03	1.10 ± 0.03	1.17 ± 0.03	1.18 ± 0.03	1.21 ± 0.08
T_{p} , keV	6.38 ± 0.37	6.25 ± 0.25	6.24 ± 0.28	6.06 ± 0.21	6.57 ± 0.58
τ_{p}	2.86 ± 0.23	3.19 ± 0.20	3.13 ± 0.21	3.38 ± 0.19	2.85 ± 0.40
$A_{\text{comp}} \times 10^1$	0.114 ± 0.002	0.142 ± 0.005	0.180 ± 0.007	0.191 ± 0.006	0.103 ± 0.007
E_{cyc1} , keV	4.88 ± 0.06	4.99 ± 0.05	5.00 ± 0.06	4.90 ± 0.06	4.61 ± 0.08
σ_{cyc1} , keV	0.75 ± 0.10	0.72 ± 0.08	0.95 ± 0.07	1.02 ± 0.10	0.87 ± 0.11
τ_{cyc1} , keV	0.30 ± 0.08	0.33 ± 0.08	0.53 ± 0.08	0.47 ± 0.12	0.42 ± 0.12
E_{cyc2} , keV	8.79 ± 0.08	9.22 ± 0.12	8.54 ± 0.05	8.39 ± 0.04	9.02 ± 0.16
σ_{cyc2} , keV	1.46 ± 0.16	1.73 ± 0.19	1.41 ± 0.09	1.09 ± 0.09	2.19 ± 0.42
τ_{cyc2} , keV	0.93 ± 0.21	0.98 ± 0.24	1.20 ± 0.15	0.91 ± 0.17	1.64 ± 0.90
E_{cyc3} , keV	—	—	—	12.56 ± 0.08	—
σ_{cyc3} , keV	—	—	—	0.64 ± 0.13	—
τ_{cyc3} , keV	—	—	—	0.28 ± 0.07	—
E_{cyc4} , keV	—	—	17.55 ± 0.22	16.86 ± 0.09	16.90 ± 0.26
σ_{cyc4} , keV	—	—	1.34 ± 0.26	0.84 ± 0.11	1.23 ± 0.35
τ_{cyc4} , keV	—	—	0.56 ± 0.13	0.58 ± 0.08	0.54 ± 0.21
C_{modB}	1.063 ± 0.006	1.067 ± 0.006	1.075 ± 0.005	1.075 ± 0.005	1.074 ± 0.007
C_{NIC}	0.933 ± 0.011	0.960 ± 0.011	0.979 ± 0.010	0.976 ± 0.010	0.917 ± 0.012
$F_X \times 10^{10}$	3.6	4.5	5.7	6.1	3.1
χ^2 (d.o.f.)	601.3 (592)	745.6 (626)	681.2 (647)	630.1 (654)	643.8 (576)

Notes. See Notes to Table 1

here k is a factor relating to the size of the magnetosphere for a given accretion configuration to the Alfvén radius and B_{12} is the magnetic field in units of 10^{12} G and L_{10} is a lowest measure bolometric flux of the source calculated in assumption of 10 kpc distance. Assuming canonical neutron star parameters of $M = 1.4M_{\odot}$, $R = 10^6$ cm and $k = 0.5$, the measured source minimal luminosity $L_{10} = 5.9 \times 10^{33}$ erg/s and the spin period of 15.4 s one obtains the magnetic field value $B_{12} \leq 1 \times d_{10}$. Considering the limits on distance from Gaia EDR3 of 5.8-12 kpc (Bailer-Jones et al. 2021), $B_{12} \leq (0.58 - 1.2) \times 10^{12}$ G. Although formally consistent with interpretation of either 4.9 keV and 9 keV lines as fundamental, the line at 9 keV is already at the edge of the allowed distance range and inconsistent with the best photo-geometric Gaia estimate of 6.6 kpc. We conclude, therefore, that also observed properties of Swift J1626.6-5156 in quiescence favor the low field implied by ~ 4.9 keV fundamental cyclotron line energy.

This makes Swift J1626.6-5156 the weakest magnetised classical X-ray pulsar among all cyclotron line sources and might have relevant consequences for the science program of upcoming X-ray polarimeters such as *IXPE* (Weisskopf et al. 2016), and the polarisation focusing array (PFA) on board the *eXTP* mission (Zhang et al. 2016; Santangelo et al. 2019). Indeed,

those instruments operate in the soft X-ray band where the emission of XRPs is expected to be strongly polarized due to the birefringence induced by a Compton scattering in the strong magnetic field (Meszaros et al. 1988) for ordinary and extraordinary mode photons. The cross-sections for photons with both modes become comparable around the cyclotron resonance energy, which makes this energy extremely interesting. For the vast majority of XRPs the cyclotron resonance energy lies outside of the operational range of the gas pixel detectors used in *IXPE*/*eXTP* polarimeters. The only exceptions are Swift J1626.6-5156 and GRO J1744-28. However GRO J1744-28 has a very low outburst duty cycle and thus it is unlikely that will be observed. On the other hand, Swift J1626.6-5156 appears to be regularly detectable by all sky monitors and wide field X-ray instruments and thus is the ideal target for the soon to come X-ray polarimeters, especially if it undergoes another giant outburst.

ACKNOWLEDGEMENTS

We thank the *NuSTAR* team for the help with organising prompt observation. This work was financially supported by the Russian Science Foundation (grant 19-12-00423).

REFERENCES

- Bailer-Jones, C. A. L., Rybizki, J., Foesneau, M., Demleitner, M., & Andrae, R. 2021, *AJ*, 161, 147
- Baykal, A., Göğüç, E., Çağdaş İnam, S., & Belloni, T. 2010, *ApJ*, 711, 1306
- Boldin, P. A., Tsygankov, S. S., & Lutovinov, A. A. 2013, *Astronomy Letters*, 39, 375
- Burderi, L., Di Salvo, T., Robba, N. R., La Barbera, A., & Guainazzi, M. 2000, *ApJ*, 530, 429
- Corbet, R. H. D. 1986, *MNRAS*, 220, 1047
- D’Aì, A., Di Salvo, T., Iaria, R., et al. 2015, *MNRAS*, 449, 4288
- DeCesar, M. E., Boyd, P. T., Pottschmidt, K., et al. 2013, *ApJ*, 762, 61
- Doroshenko, R., Santangelo, A., Doroshenko, V., Suleimanov, V., & Piraino, S. 2015, *MNRAS*, 452, 2490
- Ferrigno, C., Becker, P. A., Segreto, A., Mineo, T., & Santangelo, A. 2009, *A&A*, 498, 825
- Filippova, E. V., Tsygankov, S. S., Lutovinov, A. A., & Sunyaev, R. A. 2005, *Astronomy Letters*, 31, 729
- Gendreau, K., & Arzoumanian, Z. 2017, *Nature Astronomy*, 1, 895
- Harrison, F. A., Craig, W. W., Christensen, F. E., et al. 2013, *ApJ*, 770, 103
- Heindl, W. A., Rothschild, R. E., Coburn, W., et al. 2004, in *American Institute of Physics Conference Series*, Vol. 714, *X-ray Timing 2003: Rossi and Beyond*, ed. P. Kaaret, F. K. Lamb, & J. H. Swank, 323–330
- Ićdem, B., Inam, S., & Baykal, A. 2011, *MNRAS*, 415, 1523
- Iwakiri, W., Wolff, M., Pottschmidt, K., et al. 2021, *The Astronomer’s Telegram*, 14457, 1
- Kreykenbohm, I., Wilms, J., Coburn, W., et al. 2004, *A&A*, 427, 975
- Krimm, H., Barthelmy, S., Capalbi, M., et al. 2005, *GRB Coordinates Network*, 4361, 1
- Lutovinov, A. A., & Tsygankov, S. S. 2009, *Astronomy Letters*, 35, 433
- Lutovinov, A. A., Tsygankov, S. S., Suleimanov, V. F., et al. 2015, *MNRAS*, 448, 2175
- Markwardt, C. B., & Swank, J. H. 2005, *The Astronomer’s Telegram*, 679, 1
- Matsuoka, M., Kawasaki, K., Ueno, S., et al. 2009, *PASJ*, 61, 999

- Meszaros, P., & Nagel, W. 1985, *ApJ*, 299, 138
- Meszaros, P., Novick, R., Szentgyorgyi, A., Chanan, G. A., & Weisskopf, M. C. 1988, *ApJ*, 324, 1056
- Molkov, S., Lutovinov, A., Tsygankov, S., et al. 2021, *The Astronomer's Telegram*, 14462, 1
- Molkov, S., Lutovinov, A., Tsygankov, S., Mereminskiy, I., & Mushtukov, A. 2019, *ApJL*, 883, L11
- Nagase, F. 1989, *PASJ*, 41, 1
- Negoro, H., Nakajima, M., Iwakiri, W., et al. 2021a, *The Astronomer's Telegram*, 14454, 1
- Negoro, H., Nakajima, K. S. M., Kawai, N., et al. 2021b, *The Astronomer's Telegram*, 14498, 1
- Negueruela, I., & Smith, D. M. 2006, *The Astronomer's Telegram*, 831, 1
- Palmer, D., Barthelmy, S., Cummings, J., et al. 2005, *The Astronomer's Telegram*, 678, 1
- Pavlinisky, M., Tkachenko, A., Levin, V., et al. 2021, *arXiv e-prints*, arXiv:2103.12479
- Predehl, P., Andritschke, R., Arefiev, V., et al. 2021, *A&A*, 647, A1
- Rea, N., Testa, V., Israel, G. L., et al. 2006, *The Astronomer's Telegram*, 713, 1
- Reig, P., Belloni, T., Israel, G. L., et al. 2008, *A&A*, 485, 797
- Reig, P., Nespoli, E., Fabregat, J., & Mennickent, R. E. 2011, *A&A*, 533, A23
- Santangelo, A., Segreto, A., Giarrusso, S., et al. 1999, *ApJL*, 523, L85
- Santangelo, A., Zane, S., Feng, H., et al. 2019, *Science China Physics, Mechanics, and Astronomy*, 62, 29505
- Shtykovsky, A. E., Lutovinov, A. A., Tsygankov, S. S., & Molkov, S. V. 2019, *MNRAS*, 482, L14
- Staupert, R., Trümper, J., Kendziorra, E., et al. 2019, *A&A*, 622, A61
- Sunyaev, R., Arefiev, V., Babyshkin, V., et al. 2021, *arXiv e-prints*, arXiv:2104.13267
- Sunyaev, R. A., & Titarchuk, L. G. 1980, *A&A*, 500, 167
- Titarchuk, L. 1994, *ApJ*, 434, 570
- Tsygankov, S. S., Lutovinov, A. A., Churazov, E. M., & Sunyaev, R. A. 2007, *Astronomy Letters*, 33, 368
- Tsygankov, S. S., Lutovinov, A. A., Doroshenko, V., et al. 2016, *A&A*, 593, A16
- Tsygankov, S. S., Wijnands, R., Lutovinov, A. A., Degenaar, N., & Poutanen, J. 2017, *MNRAS*, 470, 126
- Weisskopf, M. C., Ramsey, B., O'Dell, S., et al. 2016, in *Society of Photo-Optical Instrumentation Engineers (SPIE) Conference Series*, Vol. 9905, *Space Telescopes and Instrumentation 2016: Ultraviolet to Gamma Ray*, ed. J.-W. A. den Herder, T. Takahashi, & M. Bautz, 990517
- Zhang, S. N., Feroci, M., Santangelo, A., et al. 2016, in *Society of Photo-Optical Instrumentation Engineers (SPIE) Conference Series*, Vol. 9905, *Space Telescopes and Instrumentation 2016: Ultraviolet to Gamma Ray*, ed. J.-W. A. den Herder, T. Takahashi, & M. Bautz, 99051Q